Article

Imaging sensory transmission and neuronal plasticity in primary sensory neurons with a positively tuned voltage indicator

Check for updates

Yan Zhang [1], John Shannonhouse [1], Ruben Gomez [1], Hyeonwi Son [1], Hirotake Ishida[1], Stephen Evans[2], Mariya Chavarha[3], Dongqing Shi[2], Guofeng Zhang[2], Michael Z. Lin [2,3,4] & Yu Shin Kim [1,5] ✉

Primary sensory neurons convert external stimuli into electrical signals, yet how heterogeneous neurons encode distinct sensations remains unclear. In vivo dorsal root ganglia (DRG) imaging with genetically-encoded Ca^{2+} indicators (GECIs) enables mapping of neuronal activity from over 1800 neurons per DRG in live mice, offering high spatial and populational resolution. However, GECIs' slow Ca^{2+} response kinetics limit the temporal accuracy of neuronal electrical dynamics. Genetically-encoded voltage indicators (GEVIs) provide real-time voltage tracking but often lack the brightness and dynamic range required for in vivo use. Here, we used soma-targeted ASAP4.4-Kv, a bright and fast positively tuned GEVI, to dissect temporal dynamics of DRG neuron responses to mechanical, thermal, or chemical stimulation in live male and female mice. ASAP4.4-Kv revealed previously unrecognized cell-to-cell electrical synchronization and robust dynamic transformations in sensory coding following tissue injury. Combining GEVI and GECI imaging empowers spatiotemporal analysis of sensory signal processing and integration mechanisms in vivo.

Dorsal root ganglia (DRG) neurons have pseudounipolar axons that project toward skin where they initially convert external stimuli such as touch, stretch, itch, hot, cold, and/or chemical stimuli into corresponding electrical signals. These electrical signals are integrated and modulated in the cell bodies of DRG located in intervertebral foramen between spinal vertebrae, and then the resulting action potentials containing somatosensory information are further propagated to the superficial laminae of the dorsal spinal cord. Electrophysiologic recording has been used as a fundamental tool for measuring neuronal electrical signals for many decades, but this approach is limited by the invasiveness of the procedure, poor anatomical accessibility, the absence of physiological input during commonly used in vitro recordings, and the challenges of in vivo stability[1–3]. Genetically-encoded Ca^{2+} indicators (GECIs) have emerged as a powerful tool,

allowing for monitoring DRG neuronal activation, network patterns among neurons and other cell types, and sensory circuits in physiological and pathological conditions with exceptional spatial and populational resolution and limited perturbation[4]. However, GECIs have inherent limitations. They cannot distinguish between action potential-evoked Ca^{2+} influx vs. Ca^{2+} transients arising from internal stores and ligand-gated Ca^{2+} channels. Furthermore, Ca^{2+} indicators only report suprathreshold signaling while failing to detect subthreshold membrane potential fluctuations due to slow kinetics and limited sensitivity[2,3,5].

As an alternative, genetically encoded voltage indicators (GEVIs) provide a complementary approach to in vivo GECI imaging by enabling the detection of both fast suprathreshold voltage signals and subthreshold membrane potential fluctuations. Dynamic voltage

[1]Departments of Oral and Maxillofacial Surgery, University of Texas Health Science Center at San Antonio, San Antonio, TX, USA. [2]Department of Neurobiology, Stanford University, Stanford, CA, USA. [3]Department of Bioengineering, Stanford University, Stanford, CA, USA. [4]Department of Chemical and Systems Biology, Stanford University, Stanford, CA, USA. [5]Programs in Integrated Biomedical Sciences, Translational Sciences, Biomedical Engineering, Radiological Sciences, University of Texas Health Science Center at San Antonio, San Antonio, TX, USA. ✉e-mail: kimy1@uthscsa.edu

imaging employing voltage-sensing dyes has been used for decades to study electrical activity in various tissues and organisms[6–10], but it does not allow for recording from multiple individual neurons in densely packed neuronal tissues, such as primary sensory neurons. More recently, GEVIs have enabled sparse labeling, either through random expression or targeting genetically defined subtypes[11–16]. An increasing number of GEVIs have been successfully used for in vivo optical imaging to detect voltage dynamics in the living mouse brain. These include archaerhodopsin-based indicator Ace2N, paQuasAr3-s, and SomArchon[17–19], and ASAP-family GEVIs in which a voltage-sensitive domain (VSD) is linked to a circularly permuted GFP protein[20–23].

Compared to archaerhodopsin-based GEVIs, ASAP3-Kv enables accurate tracking of both suprathreshold and subthreshold voltage dynamics with decent signal-to-noise ratio (SNR), even in deep brain regions of live mice[20,21]. However, ASAP3-Kv generates a reversed optical signal (a decrease in fluorescence intensity with membrane depolarization), which leads to high excitability and thus high photobleaching at resting membrane potentials. To overcome this limitation, positively tuned GEVIs that brighten with positive voltage changes have been engineered, using either VSDs from voltage-sensitive phosphatases (FlicR1[24,25], Marina[26], and ASAP4[22]), or from voltage-sensitive opsins (Positron[27], pAce and pAceR[28]). Among these indicators, Marina exhibits the largest optical responses in in vitro experiments, while practical use in vivo needs more evaluations. Recent attempts have successfully developed some positively tuned voltage indicators that surpass currently available positively tuned voltage indicators in their fluorescence responses and SNRs[22]. One such indicator, ASAP4.4-Kv, in which ASAP4.4 voltage indicator is attached to the Kv2.1 potassium channel to locate ASAP4.4 to the soma, combines notable properties for in vivo applications: brightening in response to membrane depolarization, high-level neuronal expression, fast kinetics, and enhanced fluorescence changes. We therefore anticipate that the properties of ASAP4.4-Kv make it more suitable and optimal for routine and robust in vivo DRG imaging, as it reliably captures action potentials and reveals subthreshold events in optical studies.

To illustrate the feasibility and utility of ASAP4.4-Kv as an indicator in primary sensory neurons, we examined neuronal activity in the DRG of live mice. Data acquired using ASAP4.4-Kv uncovered striking cell-to-cell communication and synchronization patterns between adjacent DRG neurons following peripheral inflammation or nerve injury, which were rarely seen in naïve animals. ASAP4.4-Kv imaging permitted visualizing the neuronal representation of mechanical, thermal, and chemical stimuli in vivo, and enabled us to track how these parameters transform with peripheral injury. By directly comparing in vivo GEVI and GECI signals, we found that GECI imaging effectively captures complex phenomena extending to an entire population ensemble of DRG neurons, but that images lack temporal precision and fidelity. In contrast, ASAP4.4-Kv voltage imaging enabled high-temporal-resolution visualization of individual DRG neuronal activity, allowing for a more precise assessment of fast electrical signals. We conclude that combining GEVI and GECI imaging provides an optimal approach for analyzing the complex signal processing and integration of somatosensation in various contexts.

Results

Using ASAP4.4-Kv for in vivo DRG voltage imaging

For in vivo intact DRG voltage imaging, we intrathecally injected adeno-associated viruses (AAVs) encoding ASAP4.4-Kv into the spinal cord to drive expression in DRG neurons. At 5–7 weeks after injection, in vivo single photon confocal imaging experiments were performed on the right lumbar (L5) DRG, which innervates parts of the right hindpaw, leg, and back of the mouse. Fluorescent signals from ASAP4.4-Kv were acquired by confocal microscopy in frame mode to capture the entire L5 DRG neuronal population. We verified successful

transduction of ASAP4.4-Kv virus into DRG neurons by imaging ASAP4.4-Kv fluorescence. The basal ASAP4.4-Kv green fluorescence intensity was relatively low under in vivo conditions; however, inflammation in hindpaw caused by complete Freund's adjuvant (CFA) injection or chronic constriction injury[29] of sciatic nerves (SNs) yielded a stronger ASAP4.4-Kv fluorescent signal (Fig. 1a–c and Supplementary Fig. 1a–c). The results show that ASAP4.4-Kv can be sparsely targeted to the somatic plasma membrane of DRG neurons and can dynamically respond to voltage changes within the physiological range (Supplementary Fig. 2). These are essential properties for carrying out the functional analysis at the cellular level in vivo.

We noticed that many DRG neurons showing brightly fluorescent ASAP4.4-Kv were in close proximity to each other, more prominent in CFA and SN-CCI animals (Supplementary Fig. 1c), implying that "cross-excitation[30]" or "coupled activation[4]" may arise between adjacent primary sensory neurons in vivo. This phenomenon led us to further explore the potential of voltage indicators in revealing neuronal crosstalk and network communication within the peripheral nervous system of live animals.

Electrical coupling synchronization between adjacent DRG neurons revealed by ASAP4.4-Kv

DRG neurons are covered with satellite glial cells (SGCs), grouping with or without SGCs in between neighboring neurons[31]. Under normal circumstances, DRG neurons are loosely connected to each other or to SGCs. In contrast, extensive dye transfer and electrical coupling between adjacent neurons are often observed in many pain conditions, including inflammation in mouse hindpaw and sciatic nerve injury[4,32,33], which is attributed to gap junctions present in both DRG neurons and their surrounding SGCs. As a consequence of electrical coupling by gap junction, DRG neurons exhibit coupled activation following peripheral tissue injury examined by Ca^{2+} imaging in DRG of live mice[4].

We thus attempted to simultaneously record electrical activity between two adjacent DRG neurons using ASAP4.4-Kv. We randomly selected pairs of adjacent DRG neurons in different DRG regions and performed single-line scans at about 1.1 kHz across the membrane regions of the two neuronal cells (Fig. 1a–c, images). We analyzed paired data sets from naïve, CFA, or SN-CCI animals by quantification of fluorescence intensity changes in scanned areas of individual adjacent cells. In naïve mice, very few DRG neurons displayed rhythmic spontaneous subthreshold voltage fluctuations, and no temporal cell-to-cell coherence or synchronization of membrane voltage signals was observed (Fig. 1a). Under the context of inflammation or nerve injury, subthreshold voltage fluctuations were readily detectable in vivo (Fig. 1b, c), with an approximately 10-fold increase in average area under the curve (AUC) of ASAP4.4-Kv fluorescent signal intensity (Fig. 1d). Strikingly, around 6% of recording neuronal pairs exhibited spontaneous suprathreshold (spiking) activity and strong coincident voltage changes lasting tens to hundreds of milliseconds, regardless of activity patterns (Fig. 1b, c), whereas gap junction blocker, carbenoxolone (CBX), significantly reduced cell-to-cell electrical synchronization (Fig. 1b, e, f). Our results indicate that tissue injury increased cell-to-cell connectivity and network communication between DRG neurons, leading to enhanced synchronization in DRG neuronal networks, and eventually to better integration and summation of somatosensory signals. To the best of our knowledge, such electrically synchronous neuronal events between cells in the peripheral sensory system in vivo have not been previously described.

To determine whether electrically synchronous events corresponded to global neuronal activity, we included in vivo intact DRG Ca^{2+} imaging of neuronal populations using Pirt-GCaMP3 mice, in which the GECI GCaMP3 was exclusively expressed in primary sensory neurons under the control of the *Pirt* promoter[34]. Using Pirt-GCaMP3 Ca^{2+} imaging, we could simultaneously monitor population-wide neuronal activity in the DRG[4]. Spontaneous Ca^{2+} activity was rare in naïve
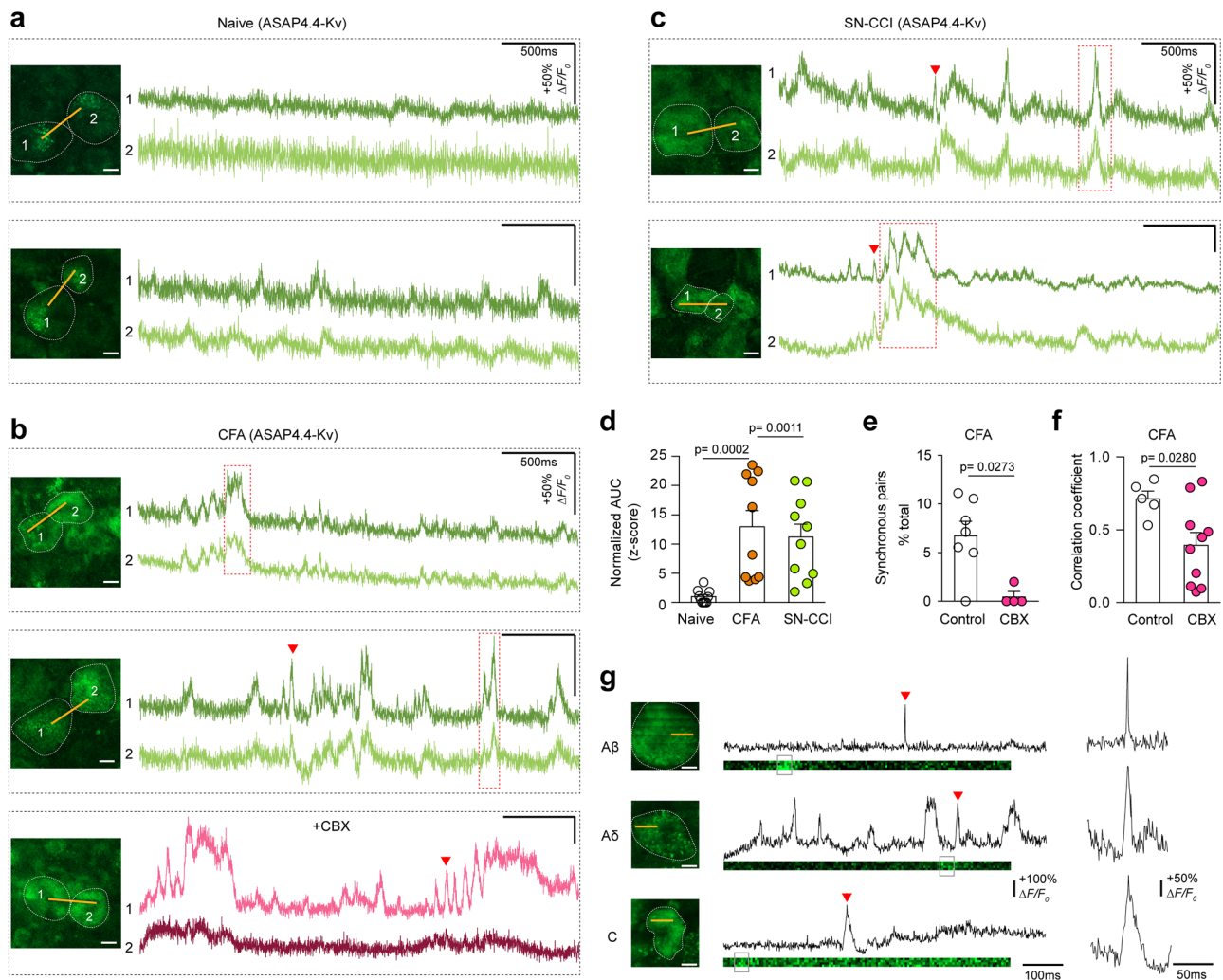
Fig. 1 | In vivo optical detection of electrically synchronous, spontaneous neuronal activity using ASAP4.4-Kv voltage imaging in intact DRG neurons. Paired optical recordings of two DRG somata (white dotted lines) expressing ASAP4.4-Kv in naïve (**a**), CFA (**b**), or SN-CCI (**c**) animals. Yellow lines indicate 1.1 kHz line scan regions where ASAP4.4-Kv fluorescent signals were acquired. In **b**, representative traces show electrical de-synchronization between a pair of adjacent DRG neurons approximately 1 hr after systemic injection of gap junction blocker, CBX (100 mg/kg, i.p.). The subthreshold voltage dynamics from recording neurons were gradually diminished following de-synchronization by gap junction blocker. The red arrow marks one of action potentials and red box indicates action potential burst. **d** Mean area under the curve (AUC) of ASAP4.4-Kv z-score signals in L5 DRG neurons from naïve, CFA, or SN-CCI animals (each dot represents an individual recorded neuron; number of cells = 10 from three biologically independent mice per group; Kruskal-Wallis test with Dunn's post-hoc test). **e** Percentage of synchronous pairs in total DRG neuron pairs recorded from CFA mice without (control) and with systemic CBX injection (each dot represents an individual CFA-treated animal; number of biologically independent CFA mice = 7 and 4 for control (without CBX treatment) and CBX-treated groups, respectively; two-tailed Mann-Whitney U-test. **f** Correlation coefficients were calculated from DRG neuron pairs recorded from CFA mice without (control) and with systemic CBX injection (each dot represents one pair of DRG neurons; number of DRG pairs = 5 and 10 for control (without CBX treatment) and CBX-treated groups, respectively, from three biologically independent mice per group; two-tailed Mann-Whitney U-test). Neuron pairs exhibit electrical correlation, whereas the correlation is dissociated by gap junction blocker. Fluorescence traces showing respiratory motion or heartbeat-like rhythmic events, or digital artifacts were not considered as electrical synchronization in the analysis. **g** Optical ASAP4.4-Kv signals from DRG neurons of different size reveal various action potential shapes, in agreement with Aβ, Aδ and C-type nociceptor properties. Grey box on the line scan image indicates regions of interest (ROI). Red arrow marks one of action potentials recorded from ROIs, with expanded view on the right. Scale bar in inset image: **a**–**c**: 10 μm. **g**: 10 μm. All data are presented as mean values ± SEM.

animals (1–3 neurons/DRG) but increased (>10 neurons/DRG) with peripheral injury (Supplementary Fig. 3a, b), though no synchronized spontaneous activity was detected. While ASAP4.4-Kv detected numerously dynamic membrane voltage signal changes associated with inflammation or nerve injury (Fig. 1d), GCaMP3 primarily reflected an increased number of spontaneously activated neurons (Supplementary Fig. 3c–e).

Noninvasive optical readout of different afferent subtypes in vivo with ASAP4.4-Kv

Primary sensory neurons diverge in function as they express their own unique receptors and ion channels. Classically, DRG neurons are categorized into three subtypes based on somatic action potential shapes and conduction velocity: myelinated Aβ low threshold-mechano-receptors (LTMRs), which are large-diameter, fast-conducting neurons; Aδ afferent nociceptor, which have medium diameter and conducting velocity; and C-type nociceptor, which are small-diameter unmyelinated and slowly conducting[35,36]. Identification and functional characterization of neuronal subtypes in vivo have been a challenge; thus, current investigations have mostly relied on the invasive in vitro or ex vivo electrophysiologic recordings[37,38]. As shown in Fig. 1g, we were able to visualize single action potentials by inspecting a small spiking area (1–3 μm) of the line scan image. We found that the kinetic properties of action potentials were closely
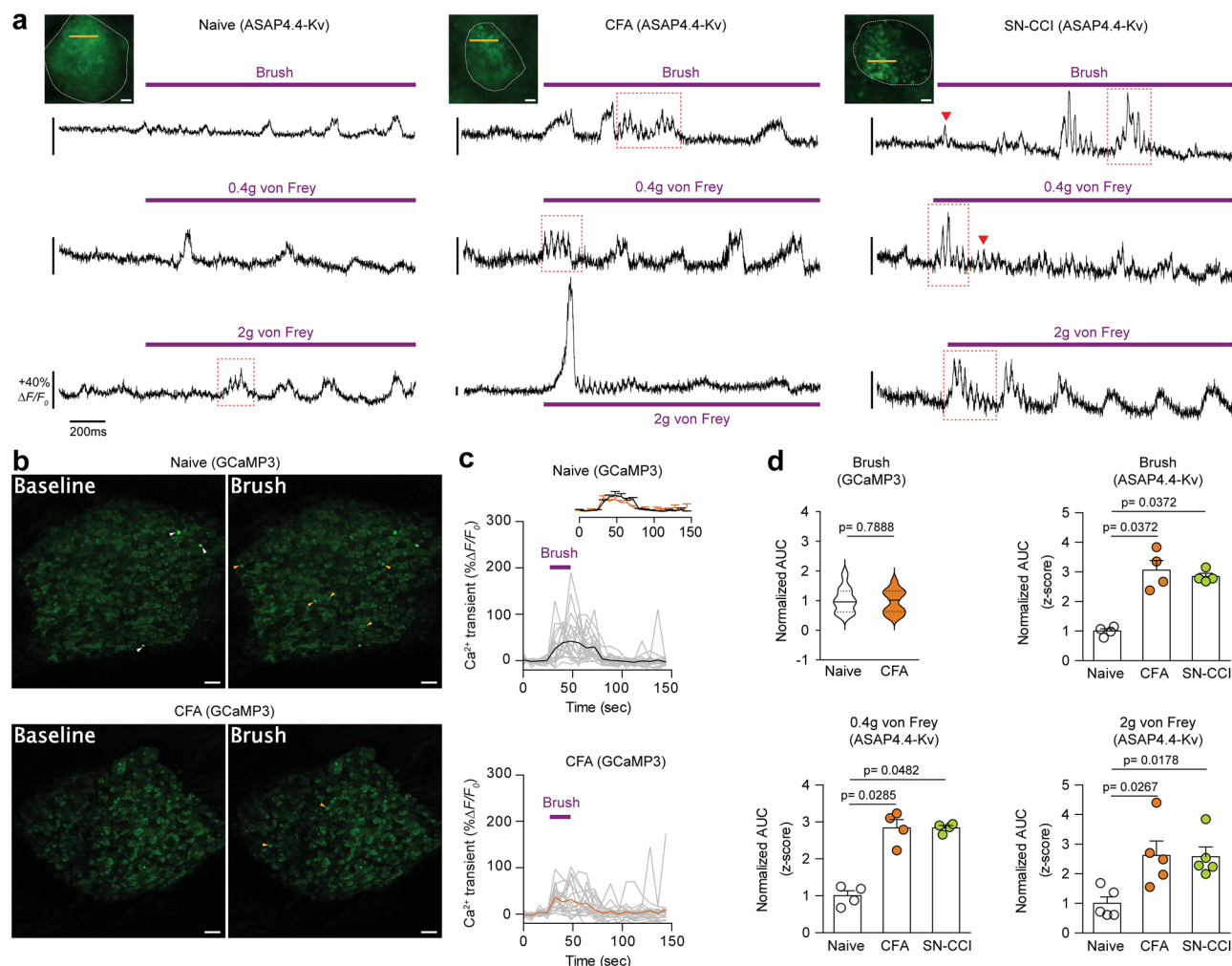
Fig. 2 | In vivo optical recording of mechanically (brush or von Frey)-induced neuronal activity in intact DRG neurons. a Optical voltage recordings of primary sensory neurons in response to the indicated stimuli in naïve, CFA, or SN-CCI animals. Purple bars indicate the timing of the stimulus application. Inset, images of DRG cell bodies (white dotted lines) expressing ASAP4.4-Kv. Yellow lines indicate 1.1 kHz line scan regions where ASAP4.4-Kv fluorescent signals were acquired. Red arrow marks one of action potentials and red box indicates action potential burst. Scale bar: 5 µm. **b** In vivo intact DRG Ca²⁺ imaging from naïve or CFA-treated Pirt-GCaMP3 mice. (*left*) Averaged images before brush stimulus was applied. (*right*) Averaged images after brush stimulus was applied. White arrowheads indicate spontaneously activated neurons without application of stimulus. Yellow arrowheads indicate DRG neurons activated by brush stimulus. Scale bar: 100 µm.

c GCaMP3 Ca²⁺ transients from individual DRG neurons (grey traces) and averaged Ca²⁺ transients (black or orange) from naïve or CFA animals. **d** Mean area under the curve (AUC) of ASAP4.4-Kv z-score signals and GCaMP3 Ca²⁺ transients in stimulated L5 DRG neurons. Brush (GCaMP3): violin plot with median (solid line) and quartiles (dashed lines); number of cells = 21 and 19 for naïve and CFA groups, respectively, from three biologically independent mice per group; two-tailed Mann-Whitney U-test. Brush and 0.4 g von Frey (ASAP4.4-Kv): each dot represents an individual recorded neuron (number of cells = 4 from three biologically independent mice per group; Kruskal-Wallis test with Dunn's post-hoc test). 2 g von Frey (ASAP4.4-Kv): each dot represents an individual recorded neuron (number of cells = 5 from three biologically independent mice per group; Kruskal-Wallis test with Dunn's post-hoc test). All data are presented as mean values ± SEM.

related to the neuron size, consistent with findings from conventional electrophysiologic recordings[37,39]. This indicates the feasibility of in vivo voltage imaging for noninvasive optical readout of electrophysiologic features, to the point where afferent subtypes can be inferred and targeted in real time.

ASAP4.4-Kv imaging permits visualization of mechanical stimuli (non-noxious to noxious)-evoked temporal summation of fast voltage signals

To understand how DRG neurons encode painful or non-painful mechanical stimuli, we applied stimulation of different strengths to the hindpaw, and visualized evoked ASAP4.4-Kv signals in DRG neurons. At low stimulation strength (light brush, 0.4 g, or 2 g von Frey; Fig. 2), small and transient subthreshold potential changes could be observed in mechanosensitive neurons (Fig. 2a), and only a few neurons exhibited hindpaw stimulation-evoked transient Ca²⁺ increases in naïve

animals (Fig. 2b). However, peripheral inflammation or nerve injury led to a significant increase in membrane electrical signal summation, including both subthreshold and suprathreshold voltage signals (Fig. 2a, d), but not in Ca²⁺ responses (Fig. 2b–d). At an intermediate stimulation strength (100 g press), high-frequency voltage dynamics were observed in neurons of naïve mice (Fig. 3a), while inflammation or nerve injury treatment produced exacerbated voltage fluctuations with larger amplitude and longer membrane depolarization (Fig. 3b–d). On the other hand, GCaMP3 Ca²⁺ imaging revealed increased population-level activities in injured mice upon exposure to the same press stimulus (Fig. 3d, e). However, large variations in the magnitude of Ca²⁺ transients were found within the same DRG and across different treatment groups. Consequently, while the data were grouped, neither average amplitudes nor the mean AUCs of Ca²⁺ transients differed significantly between naïve or injured animals (Fig. 3d, g), despite the fact that increased activated cell numbers
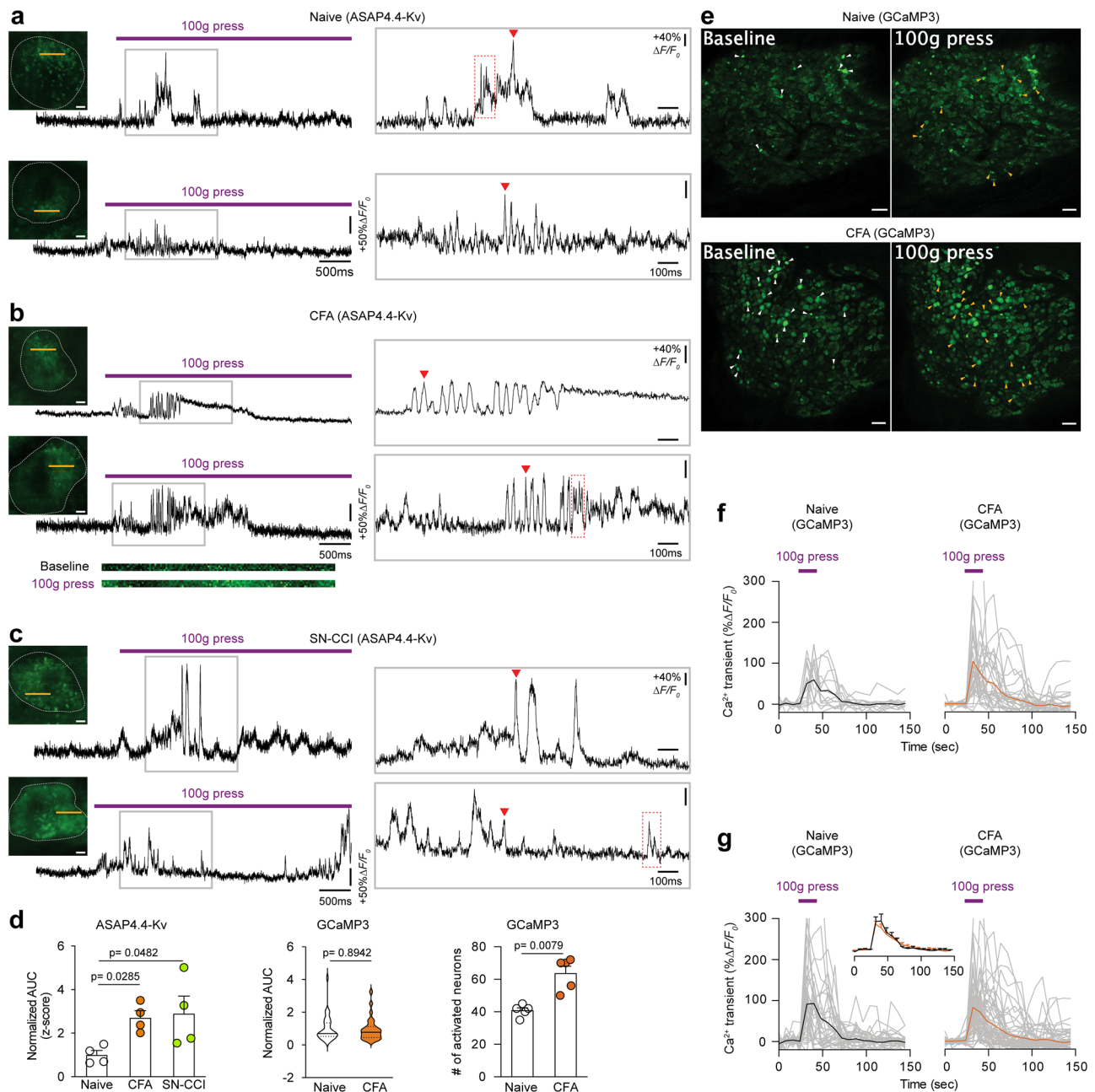
Fig. 3 | In vivo optical recording of mild press (100 g)-induced neuronal activity in intact DRG neurons. Optical voltage recordings of primary sensory neurons in response to a single mechanical force (100 g) applied to the hindpaw of naïve (**a**), CFA (**b**), or SN-CCI (**c**) animals. Insets, images of DRG cell bodies (white dotted lines) expressing ASAP4.4-Kv. Yellow lines indicate 1.1 kHz line scan regions where ASAP4.4-Kv optical recording signals were acquired. Each trace is the response of a single DRG neuron; (*right*) expanded view of the boxed region. Purple bars indicate the timing of the stimulus application. Representative line scan images in **b** are shown under the trace. Red arrow marks one of action potentials and red box indicates action potential burst. Scale bar: 5 µm. **d** Mean area under the curve (AUC) of ASAP4.4-Kv z-score signals (each dot represents an individual recorded neuron; number of cells = 4 from three biologically independent mice per group; Kruskal-Wallis test with Dunn's post-hoc test) and GCaMP3 Ca^{2+} transients (violin plot with median (solid line) and quartiles (dashed lines); number of cells = 33 and 56 for naïve and CFA groups, respectively, from three biologically independent mice per group; two-tailed Mann-Whitney U-test) in L5 DRG neurons in response to 100 g press, and the number of total activated neurons (each dot represents one animal; number of biologically independent mice = 5 per group; two-tailed Mann-Whitney U-test). **e** In vivo intact DRG Ca^{2+} imaging from naïve or CFA-treated Pirt-GCaMP3 mice. (*left*) Averaged images before application of mild press (100 g). (*right*) Averaged images after application of mild press (100 g). White arrowheads indicate spontaneously activated neurons in the absence of applied stimulus. Yellow arrowheads indicate DRG neurons activated by mild press. Scale bar: 100 µm. Ca^{2+} transients from DRG neurons in response to mild press (100 g) applied to the hindpaw using Pirt-GCaMP3 mice (grey), from one (**f**) or three (**g**) animals for each treatment. Traces of averaged Ca^{2+} transients from each group are shown in black or orange. All data are presented as mean values ± SEM.

(Fig. 3d) and increased amplitudes of Ca^{2+} transients (Fig. 3f) were evident in some CFA-injured mice.

At the strongest mechanical stimulus (300 g), long-lasting membrane potential fluctuations with sustained membrane depolarization were observed in DRG neurons of naïve mice (Fig, 4a), and voltage fluctuations in neuronal membranes were further aggravated by inflammation or nerve injury treatment (Fig. 4b, c and Supplementary movie 1). Similar to previous results, average Ca^{2+} transients differed
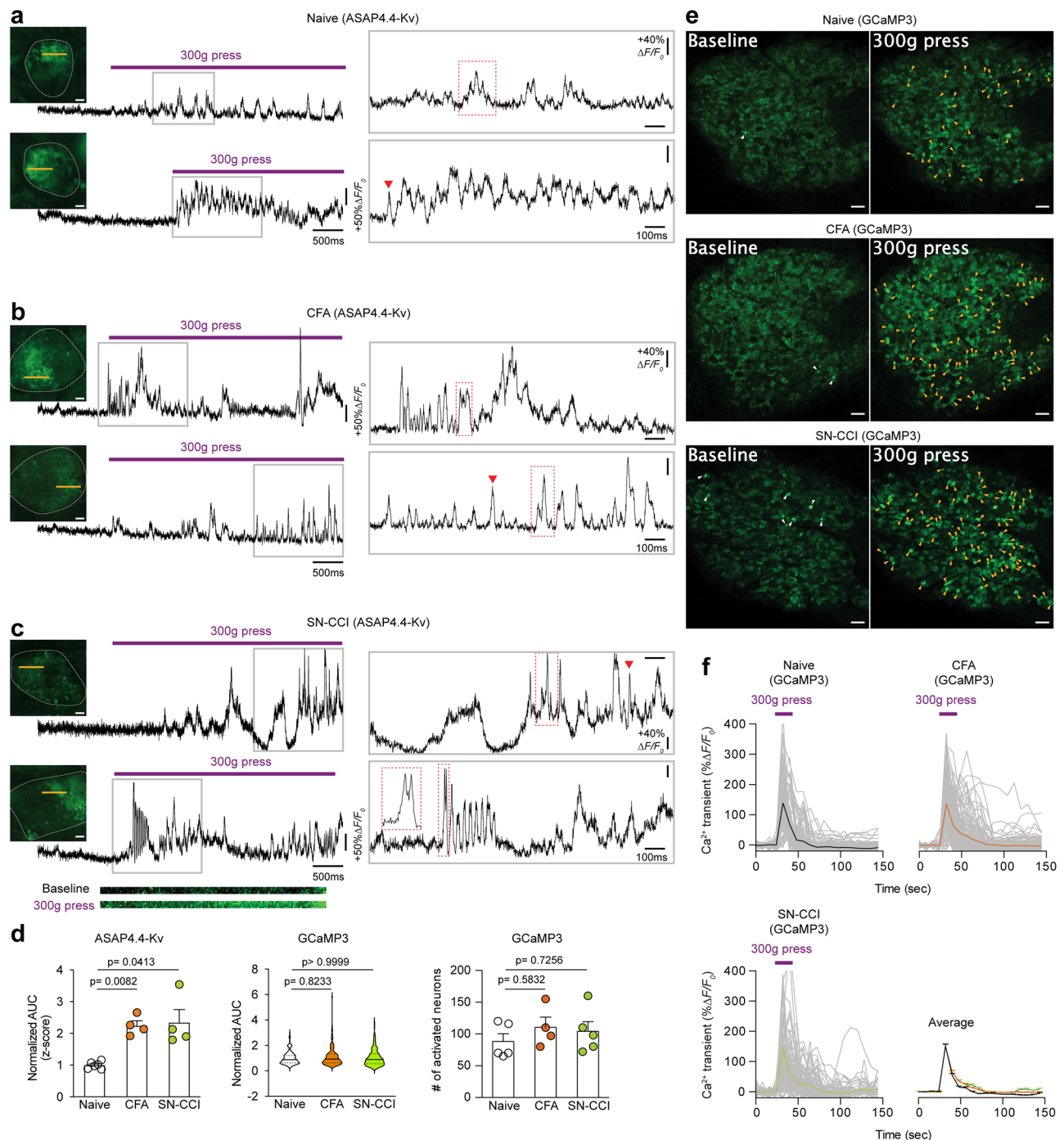
Fig. 4 | In vivo optical recording of strong press (300 g)-induced neuronal activity in intact DRG neurons. Optical voltage recordings of primary sensory neurons in response to application of a single mechanical force (300 g) to the hindpaw of naïve (**a**), CFA (**b**), or SN-CCI (**c**) animals. Insets, images of DRG cell bodies (white dotted lines) expressing ASAP4.4-Kv. Yellow lines indicate 1.1 kHz line scan regions where ASAP4.4-Kv optical recording signals were acquired. Each trace is the response of a single DRG neuron; (*right*) expanded view of the boxed region shown on the right. Purple bars indicate the timing of the stimulus application. Representative line scan images in **c** are shown under the trace. The red arrow marks one of action potentials and red box indicates action potential bursts. Scale bar: 5 μm. **d** Mean area under the curve (AUC) of ASAP4.4-Kv z-score signals (each dot represents an individual recorded neuron; number of cells = 6, 4 and 4 for naïve, CFA, and SN-CCI groups, respectively, from three biologically independent mice per group; Kruskal-Wallis test with Dunn's post-hoc test) and GCaMP3 Ca²⁺ transients (violin plot with median (solid line) and quartiles (dashed lines); number of cells = 119, 141 and 106 for naïve, CFA, and SN-CCI groups, respectively, from three biologically independent mice per group; Kruskal-Wallis test with Dunn's post-hoc test) in L5 DRG neurons in response to 300 g press, and the number of total activated neurons (each dot represents one animal; number of biologically independent mice = 5, 4 and 5 for naïve, CFA, and SN-CCI groups, respectively; Kruskal-Wallis test with Dunn's post-hoc test). **e** In vivo intact DRG Ca²⁺ imaging from naïve, CFA, or SN-CCI using Pirt-GCaMP3 mice. (*left*) Averaged images before application of strong press (300 g). (*right*) Averaged images after application of strong press (300 g). White arrowheads indicate spontaneously activated neurons in the absence of an applied stimulus. Yellow arrowheads indicate DRG neurons activated by strong press. Scale bar: 100 μm. **f** Ca²⁺ transients from DRG neurons in response to a strong press (300 g) applied to the hindpaw of Pirt-GCaMP3 mice (grey) from all naïve, CFA, or SN-CCI animals. Traces of averaged Ca²⁺ transients from each group are shown in black, orange, or green. All data are presented as mean values ± SEM.

only marginally in groups affected by inflammation or nerve injury (Fig. 4d–f), and increased numbers of activated cells were not evident (Fig. 4d and Supplementary movie 7). In addition, simultaneous in vivo dual color imaging of ASAP4.4-Kv (green) and mCyRFP3[40], a cyan-excitable red fluorescent protein that can be used as a non-perturbing voltage-independent fluorescent marker as a control signal for ASAP4.4-Kv voltage imaging, demonstrated that the pattern of evoked electrical activity was distinguishable from rhythmic physiological motions arising from respiration or heartbeat (Supplementary Fig. 4).

ASAP4.4-Kv imaging reports thermal (heat or cold)-evoked voltage signals with high temporal fidelity

It has been reported that primary sensory neurons employ different strategies to encode heat vs. cold[41,42]. To discern how heat or cold is represented in vivo, we examined the ASAP4.4-Kv voltage signals from heat or cold-sensing neurons. In naïve mice, the membrane voltage dynamics during noxious heat (50°C) stimulation displayed a slowly depolarizing voltage ramp that returned to baseline within 300 ms (Fig. 5a). Noxious cold (0°C) stimulation, however, led to two distinctive forms of voltage activity: bursting or non-bursting (Fig. 6a). Bursting neurons displayed burst-frequency firing behaviors, whereas non-bursting neurons generated only single action potentials followed by small membrane fluctuations (Fig. 6a). Inflammation or nerve injury, in turn, resulted in augmentation of membrane voltage fluctuation and electrical amplitude in both heat- and cold-sensing neurons (Fig. 5b, c and Supplementary movie 2; Fig. 6b, c and Supplementary movie 3). Notably, stimulation by heat or cold was represented by distinct populational Ca^{2+} signals under various pain conditions.

After CFA-induced inflammation, numerous DRG neurons were activated upon noxious heat stimulation (50°C) but numbers were similar between naïve and CFA groups (Fig. 5d, e and Supplementary movie 8), while fewer neurons displayed Ca^{2+} activity to noxious cold (0°C) compared to naïve animals (Fig. 6d, e). As with mechanical stimuli, heat-induced increases in Ca^{2+} transients were observed in some DRGs of individual CFA-treated mice (Fig. 5f), but not in grouped DRGs (Fig. 5d, g). In contrast, cold-sensitive neurons displayed reduced Ca^{2+} transients after peripheral inflammation, both individually (Fig. 6f) and as a group (Fig. 6d, g). These results are consistent with previous reports indicating cold-mediated Ca^{2+} activity loss in specific cold-sensing neurons following peripheral injury[42]. The discrepancy between voltage and Ca^{2+} signals in cold-sensing neurons suggests that, following peripheral inflammation, individual sensory neuron still retains the ability to encode cold stimuli, but network-level suppression in the DRG reduces the overall summation of neuronal response to painful cold.

ASAP4.4-Kv imaging reveals high potassium or capsaicin-evoked strong membrane voltage fluctuations

Finally, we used the ASAP4.4-Kv voltage sensor to examine how DRG neurons encode noxious chemical nociception. In naïve mice, direct topical application of high potassium (50 mM KCl) or capsaicin (10 μM), a TRPV1 agonist which can initiate activity in nociceptive neurons, onto L5 DRG, resulted in >4-fold increase in voltage fluctuations over baseline (Fig. 7a, d). Both CFA and SN-CCI treatments significantly increased neuronal responses to KCl or capsaicin, with substantial increases in frequency and magnitude of dynamic membrane voltage fluctuations (Fig. 7b–d and Supplementary movie 5, 6). Same chemical treatments in Pirt-GCaMP3 mice induced widespread population-level activation of DRG neurons (Fig. 7f, g). Capsaicin application primarily activated small and medium diameter neurons, which are nociceptors typically express TRPV1 receptors (Fig. 7g). On average, Ca^{2+} transients were significantly higher in injured mice than in naïve animals (Fig. 7e). Compared to physical stimulation, direct chemical administration onto DRG neurons produced near-maximal Ca^{2+} transients and responses in most DRG neurons in vivo. These findings suggest that neuronal hypersensitivity is a common consequence of peripheral injury.

Discussion

This study reports the use of an improved ASAP-family GEVI, ASAP4.4-Kv, to track both spontaneous and evoked voltage activity in mouse primary sensory neurons in vivo. ASAP4.4-Kv allows direct visualization of distinct temporal features of neuronal dynamics, subcellular voltage dynamics, plasticity induction, and neuronal coding in DRG, processes that have remained largely inaccessible and technically challenging to study in live animals. ASAP4.4-Kv's fast kinetics allow optical detection of single action potentials from individual DRG neurons, enabling noninvasive identification of somatosensory neuron subtypes in vivo without the aid of conventional invasive electrophysiological recordings. Notably, this study demonstrates in vivo electrically synchronous neuronal events in the peripheral sensory system, providing mechanistic insights into how sensory information is dynamically processed, integrated, and modulated under normal and pathological states. By providing high-speed, high-sensitivity voltage imaging, ASAP4.4-Kv serves as a powerful tool for addressing fundamental biological questions, including how primary sensory neurons encode different somatosensory modalities, how peripheral injury alters DRG neuron electrical activity and sensory coding, and how satellite glial cell-mediated gap junctions contribute to pain transmission in vivo. By answering these questions, this study significantly advances our understanding of peripheral sensory coding and underscores the potential of voltage imaging to uncover previously unrecognized mechanisms of neuronal plasticity, pain transmission, and glial-neuronal interactions.

GEVI imaging as a powerful tool complementary to GECI imaging

ASAP3-Kv, a previous ASAP family GEVI with strong responsivity and SNR for in vivo use, has a negative slope relationship between voltage and fluorescence[20,21]. In contrast, ASAP4.4-Kv produces a depolarization-dependent increase in fluorescence intensity[22], as do most GCaMP GECIs[4,34]. This positive-slope response, combined with somatic targeting and optimal brightness, greatly improves the utility of the GEVI ASAP4.4-Kv for in vivo recording of neuronal electrical signals and activity. In our in vivo intact DRG voltage sensor imaging studies, we could visualize sparse signals from the membrane surface of neuronal soma expressing fluorescent ASAP4.4-Kv with imaging depths of <20 μm below the meninges membrane. By directly comparing ASAP4.4-Kv voltage imaging with our lab previously developed GCaMP-based in vivo calcium imaging[4], We demonstrated superiority of in vivo GEVI imaging in resolving long-standing debates over the temporal attributes of neuronal coding. While GCaMP imaging is optimal for identifying neurons that respond to stimuli and assessing the total number of activated neurons, voltage imaging offers superior temporal precision and fidelity. For example, both cold and heat signals in GCaMP imaging are represented as slow Ca^{2+} transients; however, we can clearly visualize distinct patterns of cold and heat-evoked electrical activity at the single-cell level, including slow or fast depolarization, bursting or non-bursting activity, which are inaccessible by GCaMP imaging. Another advantage of GEVI imaging is the ability to examine both non-spiking (subthreshold) and spiking (action potential) electrical activity, as subthreshold membrane potential fluctuation and oscillation do not greatly affect internal Ca^{2+} levels or dynamics. ASAP4.4-Kv is able to identify non-spiking subthreshold voltage fluctuation events in DRG neurons with millisecond range resolution, an order of magnitude faster than the signal integration time of GCaMP3 or other advanced GCaMPs.

Unexpectedly, ASAP4.4-Kv voltage imaging revealed cell-to-cell coupled synchronous electrical events following injury that were normally indiscernible in GCaMP3 imaging across the DRG neuronal population. Highlighting the importance of in vivo voltage imaging,
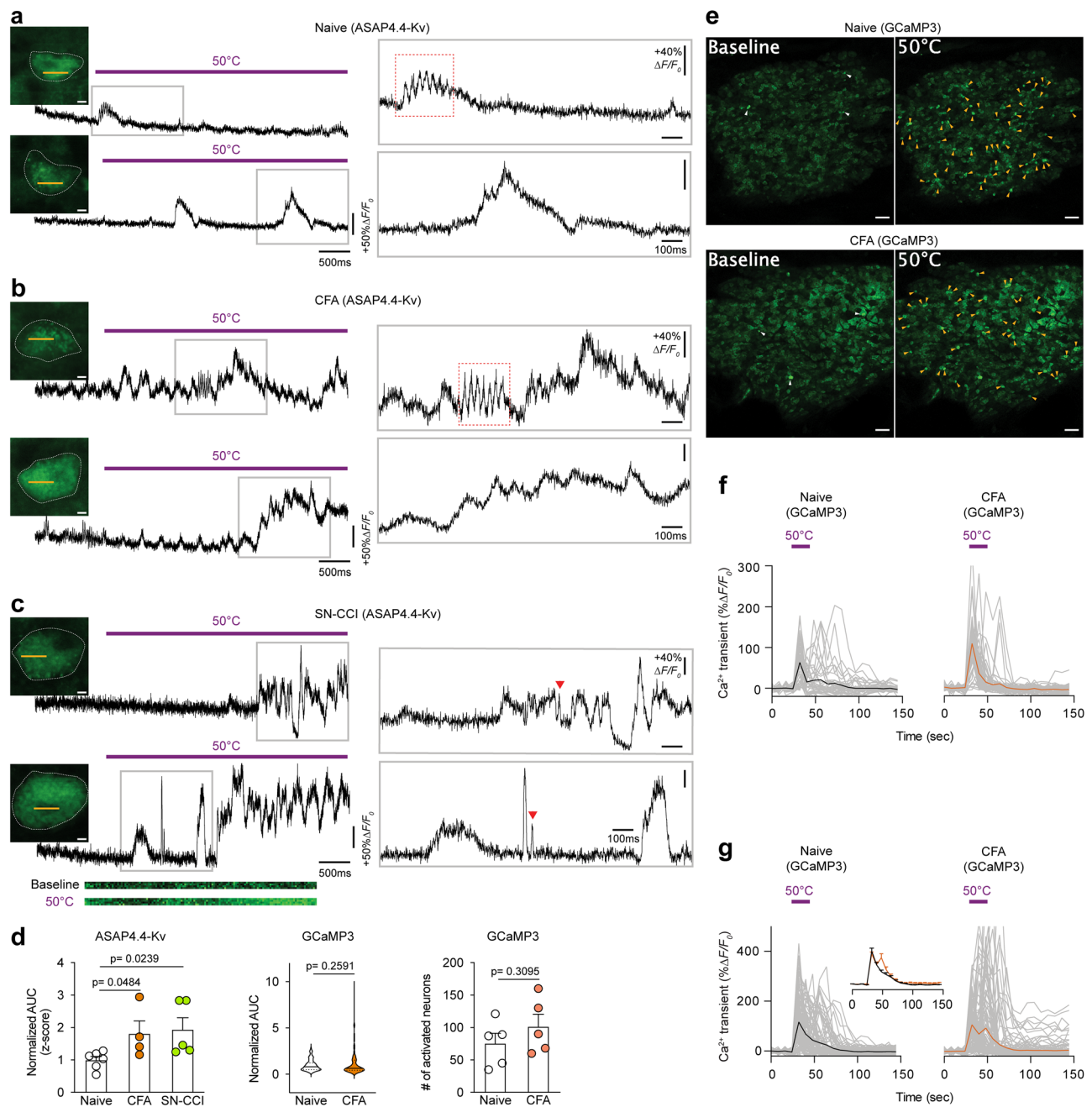
Fig. 5 | In vivo optical recording of neuronal activity in thermoreceptive neurons. Optical voltage recordings of noxious heat (50 °C)-sensitive primary sensory neurons from naïve (**a**), CFA (**b**), or SN-CCI (**c**) animals. Insets, images of DRG cell bodies (white dotted lines) expressing ASAP4.4-Kv. Yellow lines indicate 1.1 kHz line scan regions where ASAP4.4-Kv optical recording signals were acquired. Each trace is the response of a single DRG neuron; (*right*) expanded view of the boxed region. Purple bars indicate the timing of the stimulus application. Representative line scan images in **c** are shown under the trace. The red arrow marks one of the action potentials, and red box indicates action potential bursts. Scale bar: 5 μm. **d** Mean area under the curve (AUC) of ASAP4.4-Kv z-score signals (each dot represents an individual recorded neuron; number of cells = 6, 4 and 5 for naïve, CFA, and SN-CCI groups, respectively, from three biologically independent mice per group; Kruskal-Wallis test with Dunn's post-hoc test) and GCaMP3 Ca^{2+} transients (violin plot with median (solid line) and quartiles (dashed lines); number of cells = 103 and 123 for naïve and CFA groups, respectively, from three biologically independent mice per group; two-tailed Mann-Whitney U-test) in L5 DRG neurons in response to noxious heat stimulus, and the number of total activated neurons (each dot represents one animal; number of biologically independent mice = 5 per group; two-tailed Mann-Whitney U-test). **e** In vivo intact DRG Ca^{2+} imaging from naïve or CFA-treated Pirt-GCaMP3 mice. (*left*) Averaged images before application of heat stimulus (50°C). (*right*) Averaged images after application of heat stimulus (50°C). White arrowheads indicate spontaneously activated neurons in the absence of applied stimulus. Yellow arrowheads indicate DRG neurons activated by heat (50°C). Scale bar: 100 μm. Ca^{2+} transients from DRG neurons in response to heat (50°C) applied to the hindpaw of Pirt-GCaMP3 mice (grey), from one (**f**) or three (**g**) animals for each treatment. Traces of averaged Ca^{2+} transients of each group are shown in black or orange. All data are presented as mean values ± SEM.

ASAP4.4-Kv imaging fully unmasked altered DRG neuronal electrical activities and signals resulting from peripheral injury at the single-cell level in their native environment. In contrast, variable Ca^{2+} activities could be observed in in vivo Pirt-GCaMP3 Ca^{2+} imaging, but significant effects were diminished in comparisons of larger numbers of DRG neurons from multiple animals. Another fascinating aspect of fluorescence voltage sensors is their ability to map not only subthreshold depolarizing (excitatory) inputs but also hyperpolarizing (inhibitory)
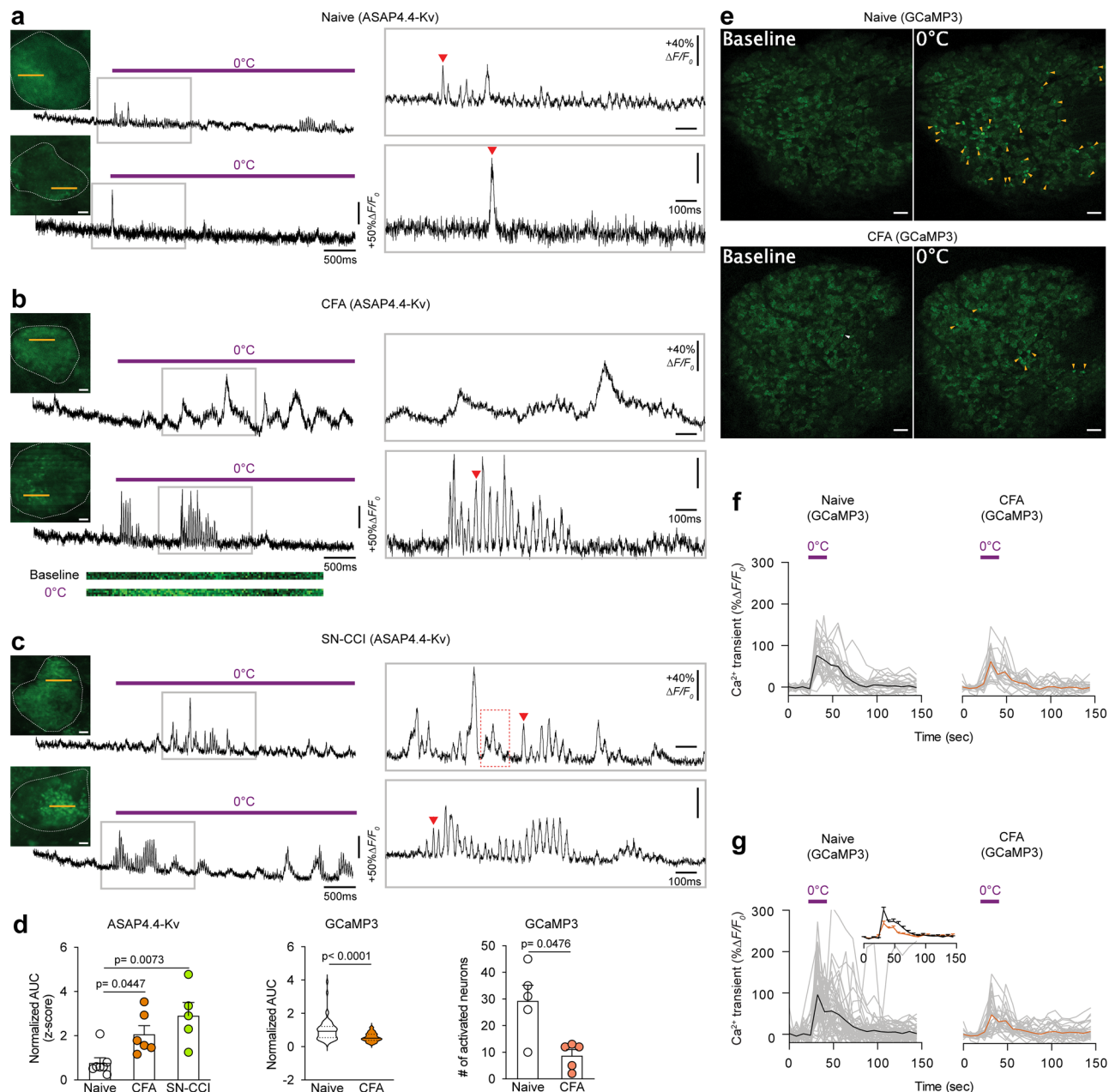
Fig. 6 | In vivo optical recording of neuronal activity in cold-sensing neurons. Optical voltage recordings of cold (0 °C)-sensitive primary sensory neurons from naïve (**a**), CFA (**b**), or SN-CCI (**c**) animals. Insets, images of DRG cell bodies (white dotted lines) expressing ASAP4.4-Kv. Yellow lines indicate 1.1 kHz line scan regions where ASAP4.4-Kv optical recording signals were acquired. Each trace is the response of a single DRG neuron; (*right*) expanded view of the boxed region. Purple bars indicate the timing of the stimulus application. Representative line scan images in **b** are shown under the trace. The red arrow marks one of the action potentials, and the red box indicates action potential bursts. Scale bar: 5 μm. **d** Mean area under the curve (AUC) of ASAP4.4-Kv z-score signals (each dot represents an individual recorded neuron; number of cells = 7, 6 and 5 for naïve, CFA, and SN-CCI groups, respectively, from three biologically independent mice per group; Kruskal-Wallis test with Dunn's post-hoc test) and GCaMP3 Ca²⁺ transients (violin plot with median (solid line) and quartiles (dashed lines); number of

cells = 58 and 34 for naïve and CFA, respectively, from three biologically independent mice per group; two-tailed Mann-Whitney U-test) in L5 DRG neurons in response to noxious cold stimulus, and the number of total activated neurons (each dot represents one animal; number of biologically independent mice = 5 per group; two-tailed Mann-Whitney U-test). **e** In vivo intact DRG Ca²⁺ imaging from naïve or CFA-treated Pirt-GCaMP3 mice. (*left*) Averaged images before application of cold stimulus (0 °C). (*right*) Averaged images after application of cold stimulus (0 °C). White arrowheads indicate spontaneously activated neurons without application of stimulus. Yellow arrowheads indicate DRG neurons activated by cold (0 °C). Scale bar: 100 μm. Ca²⁺ transients from DRG neurons in response to application of cold stimulus (0 °C) to the hindpaw of Pirt-GCaMP3 mice (grey), from one (**f**) or three (**g**) animals for each treatment. Traces of averaged Ca²⁺ transients from each group are shown in black or orange. All data are presented as mean values ± SEM.

events that occur constantly in almost all neurons[11]. Previous studies have used voltage indicators to monitor membrane hyperpolarization in cultured neurons[43], brain slices[44], or in freely moving mice[13]. The hyperpolarizing voltage signals detected by ASAP4.4-Kv in our DRG recordings were evident in response to strong stimuli, appearing as a

fluorescence intensity drop below the pre-stimulation baseline. In contrast, GECI imaging can only detect excitatory inputs, and lacks the ability to detect signals related to inhibitory inputs. Thus, a plausible use of GEVI imaging would be to examine inhibitory signaling mechanisms that regulate peripheral nociceptive or non-nociceptive
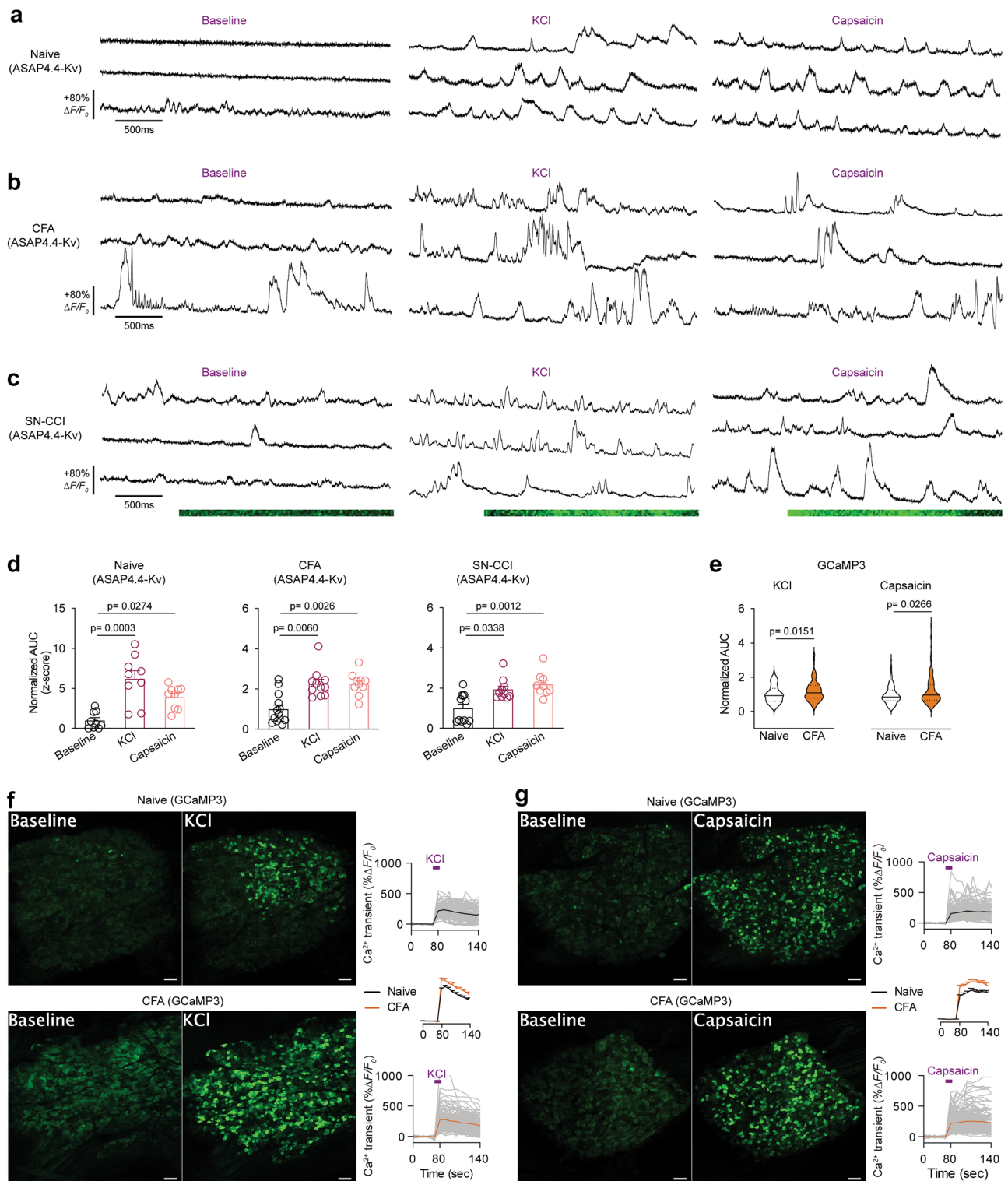
transmission, as well as to examine the summation and integration of excitatory and inhibitory signals within sensory ganglia.

Given the heterogeneity of sensory neurons, capturing integrated signals from large-scale DRG populations with high spatiotemporal resolution is essential for understanding cell-type or modality-specific coding strategies. The intrinsic slow kinetics of GECIs permits mapping large neuronal assemblies in their native environments with conventional confocal microscopic approaches. Extensive studies using GECIs have characterized sensory coding for heat or cold[41,42,45,46], mechanical[45,47,48], and chemical stimuli[49] in health and disease conditions. Due to the intrinsic fast kinetics of GEVIs, simultaneous imaging

of dozens, hundreds, or thousands of DRG neurons at high spatial (millimeters) and temporal (milliseconds) resolution is a challenging task and is limited by current technological advances. To overcome these limitations, we adapted a conventional, cost-effective, high-intensity upright laser-scanning confocal microscope into a versatile platform that enables dynamic neuronal activity recording in DRG neurons at high spatial and temporal resolution by combining GECI-based Ca^{2+} signals and GEVI-based voltage signals. With the continuous advances in voltage indicators and optical instruments, simultaneous voltage recording of enormous numbers of neurons in live intact peripheral tissues will enable dissecting functional connectivity in DRG

Fig. 7 | In vivo optical recording of intact DRG neurons in response to application of chemical stimuli (high potassium or capsaicin). Representative traces of optical voltage recordings of primary sensory neurons before (baseline) and after topical application of KCl (50 mM) or capsaicin (10 μM) to L5 DRG from naïve (**a**), CFA (**b**), or SN-CCI (**c**) animals. Representative line scan images in **c** are shown under the traces. **d** Mean area under the curve (AUC) of ASAP4.4-Kv z-score signals (each dot represents an individual recorded neuron; Naïve: number of cells = 9 for baseline, KCl, and capsaicin conditions. CFA: number of cells = 13, 11, and 10 for baseline, KCl, and capsaicin conditions, respectively. SN-CCI: number of cells = 12, 1,0 and 9 for baseline, KCl, and capsaicin conditions, respectively. Data were obtained from three biologically independent mice per group; Kruskal-Wallis test with Dunn's post-hoc test). **e** AUC of GCaMP3 Ca²⁺ transients in L5 DRG neurons in response to indicated chemical stimuli (violin plot with median (solid line) and quartiles (dashed lines); KCl: number of cells = 105 and 129 for naïve and CFA groups, respectively. Capsaicin: number of cells = 166 per group. Data were obtained from three biologically independent mice per group; two-tailed Mann-Whitney U-test). In vivo intact DRG Ca²⁺ imaging from naïve or CFA-treated Pirt-GCaMP3 mice. (*left*) Averaged images before application of indicated chemical stimuli. (*middle*) Averaged images after application of indicated chemical stimuli. Neurons activated by KCl or capsaicin are highlighted by bright fluorescence signals. Scale bar: 100 μm. (*right*) Ca²⁺ transients (gray traces) from DRG neurons in response to topical application of KCl (**f**) or capsaicin (**g**) onto DRG neurons from naïve or CFA-treated Pirt-GCaMP3 mice. Traces of averaged Ca²⁺ transients from each group are shown in black or orange. All data are presented as mean values ± SEM.

circuits and mapping neuronal coding strategies with better high-throughput and greater accuracy.

Future outlook

We previously described the phenomenon of coupled neuronal activation within DRG in mouse models of inflammatory and neuropathic pain, which is attributed to an injury-induced increase of gap junctions[4]. Here, our in vivo voltage imaging results provide evidence of gap-junction-mediated electrically synchronous neuronal activity between DRG neurons, further supporting increased neuronal 'cross talk' by gap junctions as an underlying mechanism in the development of hyperalgesia and allodynia. In our ongoing work, we aim to elucidate the precise pathways and mechanisms of neuron-to-neuron transmission.

To validate our findings, we employed multiple positive-tuned voltage indicators (ASAP4.4-Kv, Marina[26] and pAce-Kv[28]) with distinct molecular structures. All three GEVIs consistently showed enhanced voltage dynamics in DRG neurons from CFA and SN-CCI mice (Supplementary Fig. 5). Further characterization of DRG voltage activity using advanced GEVIs could offer improved temporal resolution and deeper insight into sensory neuron coding and signaling.

Our current implementation combining both GEVI and GECI imaging should allow detailed investigations of the relationship between suprathreshold somatic voltage signals and the corresponding Ca²⁺ dynamics at single-cell-, population-, or modality-specific levels. Simultaneous sub-millisecond voltage and Ca²⁺ imaging using a voltage-sensitive dye and GECI has been performed on Purkinje neurons in awake animals, and has demonstrated high spatiotemporal variations of suprathreshold voltage signals and Ca²⁺ transients between dendritic segments[50]. For in vivo primary sensory neuron studies, dual GEVI and GECI neuronal labeling with different fluorescence spectra will help in the analysis of correlation or integration between suprathreshold voltage signals and the resulting Ca²⁺ transients at high spatiotemporal resolution.

Limitations of this study

As an advanced ASAP-family sensor, positively tuned ASAP4.4-Kv demonstrated brightness, relative fluorescence change values, and SNR comparable to the previously used negatively tuned ASAP3-Kv. To enrich the fluorescence in cell bodies and reduce signals from out-of-focus neurites, Kv2.1 segment was added to the sensors for imaging in the mouse brain. Although the fluorescence level of ASAP4.4-Kv observed in the DRG was lower than that in the brain[22], we demonstrated that the density of ASAP4.4-Kv in the DRG plasma membrane is sufficient to produce a large fluorescence response. Indeed, we observed larger spiking signals (>100% $\Delta F/F_O$, Fig.1g) with ASAP4.4-Kv in DRG neurons compared to those previously observed in rodent brain in vivo (~40% $\Delta F/F_O$)[22]. It should also be noted that primary sensory neurons are nearly silent without external stimulations, which can contribute to the weak basal ASAP4.4-Kv fluorescence. Despite ASAP4.4-Kv has proven successful for in vivo DRG voltage imaging, ASAP4.4-Kv is intrinsically less photostable compared to ASAP3-Kv and therefore not well suited for long-term imaging.

ASAP4.4-Kv with optimal fluorescence response and SNR enables identifying and tracking each suprathreshold voltage spike during the designated time in our in vivo DRG recording. In two-photon optical imaging in deep layers of in vivo brain, ASAP3-Kv reliably detected single spikes and resolved spikes in bursts, with appreciable optical spike amplitudes[20]. However, in our in vivo DRG studies, each optical trace displayed in response to different stimuli is a spatial average of voltage signals from the entire line scan encompassing a surface region of 16 μm × 0.5 μm. Spatial averaging can greatly improve the SNR in optical measurements and captures more dynamic signals occurring on the cell membrane, while failing in resolving closely spaced spikes. A few spikes were detectable from a close examination of spiking activity in a small recording region. From their characteristics, we were able to identify specific cell types of primary sensory neurons and their physiological firing patterns in intact living tissues.

Another limitation of our study is the use of viruses to transduce the ASAP4.4-Kv gene into DRG neurons. Viral vectors can be used in a variety of species and for cell type-specific expression, while gene delivery via virus injection can lead to uneven expression levels depending on the injection site and imposes a limited time window of optimal expression[5,51,52]. Transgenic animals should overcome these limitations as demonstrated by our studies using the *Pirt* promotor to selectively drive strong GCaMP3 expression in DRG neurons[4]. Currently, transgenic mouse lines expressing the GEVI have been reported for in vivo studies in olfactory cells[15]. Future engineering efforts could focus on generating transgenic GEVI mouse lines for targeted tissue expression, which would promise spatially homogeneous transgene expression and long-term time windows for GEVI imaging.

In conclusion, ASAP4.4-Kv voltage imaging opens new avenues to explore the basic principles of DRG neuron coding, and of the cellular basis for perceptual changes in somatosensation by providing high temporal resolution of individual neurons. The combination of GEVI and GECI imaging allows a more temporally and spatially precise characterization of the neuronal coding and integration strategies in the peripheral somatosensory system.

Methods
Animal models

All experiments were performed in accordance with a protocol approved by the Institutional Animal Care and Use Committee at University of Texas Health Science Center at San Antonio (UTHSA). C57BL/6 J mice (body weight 20–30 g) were obtained and bred in-house. Animals were group housed unless otherwise noted, provided with food and water ad libitum, and kept on a 14/10 light/dark cycle at 23 °C. To generate CFA inflammatory injury mice, we made a 1:1 mixture of complete Freund's adjuvant (CFA): saline, and injected 50 μL subcutaneously into the glabrous skin of the hindpaw. In vivo imaging was performed 1–3 days following CFA injection. To generate sciatic nerve (SN) chronic constriction injury[29], mice were anesthetized by intraperitoneal (i.p.) injection of ketamine/xylazine (0.1/0.015 mg/g body weight). SN was exposed mid-thigh by a small incision and separated from the surrounding tissue. Ligatures were loosely tied

using 3-0 silk thread around SN. The incision was closed using sutures, and mice were used for in vivo imaging 7–10 days later. Both male and female mice were used for all experimental groups.

Pirt-GCaMP3 mice were generated by targeted homologous recombination to replace the entire coding region of the *Pirt* gene with the GCaMP3 sequence in frame with the *Pirt* promoter[4,34].

ASAP4.4-Kv virus delivery
AAV8-hSyn-ASAP4.4-Kv and AAV8-hSyn-ASAP4.4-Kv-mCyRFP3.WPRE[22] was generated by the Stanford Viral Core. For the experiments in cell culture, male or female 2 to 3-week-old mice were used for intrathecal virus delivery to DRG neurons. For in vivo imaging, 2 to 4-month-old mice of both sexes were used for intrathecal delivery of virus to peripheral neurons. For intrathecal delivery, mice of both sexes were first anesthetized with isoflurane, shaved, and disinfected. The AAVs were diluted in sterile, isotonic saline. A volume of 30 μl containing 2×10^{12} virus particles/ml was injected intrathecally (i.t.) by direct lumbar puncture using a 28½-gauge needle and insulin syringe (Becton Dickinson, Franklin Lakes, NJ). A reflexive flick of the tail indicated proper needle entry location for intrathecal injection. Following the injection, the animals were returned to recovery cages where they remained for 5–7 weeks until imaging or electrophysiology experiments were performed.

DRG exposure surgery
DRG exposure surgery was carried out to expose the intact L5 DRG. Mice were anesthetized with an i.p. injection of ketamine/xylazine (0.1/0.015 mg/g body weight). Mice were kept on a heating pad to maintain body temperature at $37 \pm 0.5°C$, which was monitored by a rectal probe. Their backs were shaved, and ophthalmic ointment was applied to their eyes to prevent drying. The transverse processes of lumbar L5 were exposed, and the surface aspect of the bone covering the DRG was carefully removed to expose the underlying DRG without damaging the DRG or spinal cord. Bleeding was gently stopped using styptic cotton or gel foam.

In vivo imaging
For in vivo imaging of the whole L5 DRG, mice were placed on a custom-built tilted stage and their spines were secured with custom-built clamps to minimize movement due to breathing and heartbeat. The stage was affixed under an LSM 800 confocal laser-scanning microscope (Carl Zeiss, Inc.) equipped with upright 5×, 10×, and 40× objectives. The isoflurane-anesthetized animals (1%–2%, vol/vol in 100% O_2) were maintained at $37 \pm 0.5°C$ by a heating pad during the imaging process. Z-stack imaging, which can cover the entire L5 DRG, was typically acquired at eight to ten frames using a 10× C Epiplan-Apochromat objective (0.4-NA, 5.4-mm free working distance, Carl Zeiss) at typically 512×512 pixel resolution with lasers tuned at 488 nm and at 561 nm and emission at 500–550 nm for green and 620–700 nm for red fluorescence. DRG neurons were at the focal plane, and imaging was monitored during the activation of DRG neuron cell bodies by peripheral hindpaw stimuli.

For the recording of ASAP4.4-Kv fluorescent signals, z-stack imaging was first performed to localize the individual spiking neurons that responded to peripheral hindpaw sensory stimuli. Next, bidirectional line scanning along neuronal cell bodies was performed on the chosen cell to achieve fast ASAP4.4-Kv imaging at 1.1 kHz. To achieve the best SNR, brighter membrane regions were selected for our line scan imaging. Respiratory motion or heartbeat-like artifacts are shown as rhythmic fluctuations, which can be removed or reduced by adjusting the z-axis depths. With increasing imaging depth, larger magnitudes of rhythmic fluctuations arising from motion artifacts were observed. When time-lapse imaging was acquired at imaging depths of <20 μm below the meninges membrane, perturbations can be greatly reduced and do not affect our results. After adjusting focus depths to avoid artifacts of membrane motion, around 7700 lines (7 s) at <1 ms per line,

128×4 pixels in image size, and 0.12 μm in pixel size were acquired per stimulus. For reporting cell-to-cell communication, around 5500 lines (5 s) at <1 ms per line were imaged at 1024 × 1 pixels in image size and 0.02 μm in pixel size. Fluorescent signals of each line were integrated to produce a movie file of fluorescent trace over time. For ASAP4.4-Kv signal analysis, the first 500–2000 lines were typically discarded due to photobleaching, and fluorescent traces with strong motion artifacts were also excluded in the analysis.

Stimulus delivery during imaging experiments
Mechanical or thermal stimuli were applied on the ipsilateral hindpaw in the following order: brush, 0.4 g von Frey, 2 g von Frey, 100 g press, 300 g press, heat (50 °C), or cold (0 °C). Paw stimuli with 100 g or 300 g press force were delivered using a rodent pincher analgesia meter, and press force was controlled manually by the experimenter. For the ASAP4.4-Kv imaging, the duration of the external stimuli was 4–5 s after 2–3 s of baseline imaging. For the GCaMP3 imaging, a time series of a total of 20 cycles was performed for each stimulus. The first 5 cycles (40–50 s) of z-stack images were captured for baseline activity determination, and images for another 5 cycles (40–50 s) were taken when paw or DRG stimuli were applied. Images were continuously taken for a total of 20 cycles. At the end of experiments, 20 μl of 50 mM KCl or 10 μM capsaicin was applied dropwise to the L5 DRG following 5 cycles of baseline imaging. After an incubation period of 1–2 cycles (5–10 s), KCl or capsaicin solution was removed by Kimwipe tissue, and then an additional 5 cycles of images were captured. Each stimulus was separated by an interval of 3–10 mins resting time for mice to avoid sensitization of neurons.

DRG culture
ASAP4.4-Kv-transduced mice of either sex (6–7 weeks old, 4 weeks after intrathecal delivery of AAV8-hSyn-ASAP4.4-Kv virus) were anesthetized with isoflurane, and euthanized by decapitation. DRG were removed bilaterally at L3–L5 and incubated in collagenase (Worthington) and dispase (Sigma-Aldrich) for 40 min at 37 °C with gentle agitation every 10 min. The dissected DRG neurons were then triturated, centrifuged, and resuspended in Dulbecco's Modified Eagle Medium (DMEM, Gibco, Grand Island, NY) supplemented with 10% fetal bovine serum (FBS, Gibco), 100 ng/ml nerve growth factor (NGF, Harlan, Indianapolis, IN), 1% penicillin/streptomycin (Gibco), and 1% L-glutamine (Gibco), and then placed on coverslips coated with poly-D-lysine and laminin (Corning, Corning, NY). Cultures were maintained at 37 °C, 5% CO_2 for 24 hr prior to electrophysiologic recordings.

In vitro electrophysiologic recording and green fluorescence imaging with ASAP4.4-Kv
Whole-cell patch-clamp recordings were performed under voltage-clamp mode using an Muticlamp 700B amplifier and pClamp11 software (Molecular Devices), and data were digitized using an Axon Instruments Digitizer. Pipette membrane capacitance was compensated, and currents were sampled at 10 kHz. Glass pipettes (3–4 MΩ resistance, World Precision Instruments (Sarasota, FL)) were filled with an intracellular solution containing the following: 140 mM K-gluconate, 5 mM KCl, 10 mM HEPES, 5 mM $MgCl_2$, 4 mM Mg-ATP, 0.3 mM Na-GTP, pH 7.2. The coverslips containing DRG neurons were transferred to the recording chamber and continuously perfused with recording solution containing: 125 mM NaCl, 2.5 mM KCl, 2 mM $CaCl_2$, 1 mM $MgCl_2$, 1.5 mM NaH_2PO_4, 15 mM $NaHCO_3$, and 10 mM D-glucose (pH 7.4), and bubbled with 5% CO_2/95% O_2.

Fluorescence traces were acquired with cells using whole-cell voltage-clamp mode. Step voltage was applied to change the membrane potential from a holding voltage of −70 mV to command voltages at −100, −40, +30, or +100 mV in a series of subsequent steps for 0.5–1 s. ASAP4.4-Kv expressing DRG neurons were imaged on an upright Zeiss Examiner.A1 microscope fitted with a 40× water-

immersion objective (0.75-NA, 2.1-mm free working distance, Carl Zeiss) and with an Axiocam 705 color camera (Carl Zeiss). Images were sampled at 5 Hz.

In vivo imaging data analysis

To analyze confocal line-scan imaging of ASAP4.4-Kv, fluorescence imaging data were extracted from raw image data, and time-dependent fluorescence traces for each neuron were revealed using the Mean ROI function in Zen Blue software. Because presentation of peripheral stimuli evoked spatially differentiated, large optical signals that were distinguishable from the stimulus-independent component, we averaged the first 1–2 s before the stimulus onset and designated that as the baseline fluorescence (F_O). Baseline-normalized amplitudes in the region of interest (ROI) over time were expressed as $(F - F_O)/F_O \times 100\%$ against time. Some experiments were excluded if the rundown exceeded 30%. To quantify evoked ASAP4.4-Kv signals that have different pre-stimuli baselines, baseline-normalized amplitudes over time were first z-scored, and area under curve (AUC) of z-scored values was then obtained using the z-score and AUC functions in GraphPad Prism.

In our analysis, only voltage transients that meet our stringent criteria are considered as single spikes: (1) sharp waveform (spiky) characteristics; (2) homogeneous shapes and time courses; (3) fast transients with temporal duration only lasting <80 ms. Subthreshold voltage changes have very slow rise and decay phases that persist for hundreds of milliseconds, and spiking activity normally occurred at the peak of subthreshold dynamics. Typically, single spikes in Aβ fiber neurons last only ~10 ms, and the spike durations increase to ~30 ms and ~50 ms in Aδ and C fiber neurons, respectively.

For GCaMP3 imaging data analysis, individual responding neurons were verified by visual examination and confirmed when the fluorescent intensity of the ROI during stimulus was 15% higher than baseline signals using the Mean ROI function in Zen blue software. Time series recorded fluorescence changes were exported to Excel and analyzed using GraphPad Prism. The average fluorescence intensity in the baseline period was taken as F_O, and was measured as the average pixel intensity during the first two to five frames of each imaging experiment. Relative change in fluorescence intensity was measured using the formula $\Delta F/F_O$ (%) $= (F - F_O)/F_O \times 100\%$.

Statistical methods

Group data were expressed as mean ± standard error of the mean (S.E.M.). Student's unpaired t-tests, Mann-Whitney U-tests, one-way ANOVA with a post-hoc Dunnett's t-test, or Kruskal-Wallis test, as appropriate, were employed for comparisons. A two-tailed p value < 0.05 was considered statistically significant for all analyses. All statistical tests are indicated in figure legends.

Reporting summary

Further information on research design is available in the Nature Portfolio Reporting Summary linked to this article.

Data availability

All data supporting the findings of this study are included in the main text and/or Supplementary Information. Source data are provided with this paper.

References

1. Anderson, M., Zheng, Q. & Dong, X. Investigation of pain mechanisms by calcium imaging approaches. *Neurosci. Bull.* **34**, 194–199 (2018).
2. Antic, S. D., Empson, R. M. & Knöpfel, T. Voltage imaging to understand connections and functions of neuronal circuits. *J. Neurophysiol.* **116**, 135–152 (2016).
3. Lin, M. Z. & Schnitzer, M. J. Genetically encoded indicators of neuronal activity. *Nat. Neurosci.* **19**, 1142–1153 (2016).
4. Kim, Y. S. et al. Coupled activation of primary sensory neurons contributes to chronic pain. *Neuron* **91**, 1085–1096 (2016).
5. Chen, T. W. et al. Ultrasensitive fluorescent proteins for imaging neuronal activity. *Nature* **499**, 295–300 (2013).
6. Cohen, L. B. et al. Changes in axon fluorescence during activity: molecular probes of membrane potential. *J. Membr. Biol.* **19**, 1–36 (1974).
7. Fujii, S., Hirota, A. & Kamino, K. Optical signals from early embryonic chick heart stained with potential sensitive dyes: evidence for electrical activity. *J. Physiol.* **304**, 503–518 (1980).
8. Loew, L. M., Cohen, L. B., Salzberg, B. M., Obaid, A. L. & Bezanilla, F. Charge-shift probes of membrane potential. Characterization of aminostyrylpyridinium dyes on the squid giant axon. *Biophys. J.* **47**, 71–77 (1985).
9. Fukunishi, K., Murai, N. & Uno, H. Dynamic characteristics of the auditory cortex of guinea pigs observed with multichannel optical recording. *Biol. Cyber* **67**, 501–509 (1992).
10. Cha, M. H. et al. Modification of cortical excitability in neuropathic rats: a voltage-sensitive dye study. *Neurosci. Lett.* **464**, 117–121 (2009).
11. Knopfel, T. & Song, C. Optical voltage imaging in neurons: moving from technology development to practical tool. *Nat. Rev. Neurosci.* **20**, 719–727 (2019).
12. Dimitrov, D. et al. Engineering and characterization of an enhanced fluorescent protein voltage sensor. *PLoS One* **2**, e440 (2007).
13. Marshall, J. D. et al. Cell-type-specific optical recording of membrane voltage dynamics in freely moving mice. *Cell* **167**, 1650–1662.e1615 (2016).
14. Kannan, M. et al. Fast, in vivo voltage imaging using a red fluorescent indicator. *Nat. Methods* **15**, 1108–1116 (2018).
15. Platisa, J. et al. Voltage imaging in the olfactory bulb using transgenic mouse lines expressing the genetically encoded voltage indicator ArcLight. *Sci. Rep.* **12**, 1875 (2022).
16. Daigle, T. L. et al. A suite of transgenic driver and reporter mouse lines with enhanced brain-cell-type targeting and functionality. *Cell* **174**, 465–480.e422 (2018).
17. Gong, Y. et al. High-speed recording of neural spikes in awake mice and flies with a fluorescent voltage sensor. *Science* **350**, 1361–1366 (2015).
18. Adam, Y. et al. Voltage imaging and optogenetics reveal behaviour-dependent changes in hippocampal dynamics. *Nature* **569**, 413–417 (2019).
19. Piatkevich, K. D. et al. Population imaging of neural activity in awake behaving mice. *Nature* **574**, 413–417 (2019).
20. Villette, V. et al. Ultrafast two-photon imaging of a high-gain voltage indicator in awake behaving mice. *Cell* **179**, 1590–1608.e1523 (2019).
21. Wu, J. et al. Kilohertz two-photon fluorescence microscopy imaging of neural activity in vivo. *Nat. Methods* **17**, 287–290 (2020).
22. Evans, S. W. et al. A positively tuned voltage indicator for extended electrical recordings in the brain. *Nat. Methods* **20**, 1104–1113 (2023).
23. Cornejo, V. H., Ofer, N. & Yuste, R. Voltage compartmentalization in dendritic spines in vivo. *Science* **375**, 82–86 (2022).
24. Abdelfattah, A. S. et al. A bright and fast red fluorescent protein voltage indicator that reports neuronal activity in organotypic brain slices. *J. Neurosci.* **36**, 2458–2472 (2016).
25. Milosevic, M. M., Jang, J., McKimm, E. J., Zhu, M. H. & Antic, S. D. In Vitro Testing of Voltage Indicators: Archon1, ArcLightD, ASAP1, ASAP2s, ASAP3b, Bongwoori-Pos6, BeRST1, FlicR1, and Chi-VSFP-Butterfly. *eNeuro* **7**, ENEURO.0060-20.2020 (2020).
26. Platisa, J., Vasan, G., Yang, A. & Pieribone, V. A. Directed evolution of key residues in fluorescent protein inverses the polarity of voltage sensitivity in the genetically encoded indicator ArcLight. *ACS Chem. Neurosci.* **8**, 513–523 (2017).
27. Abdelfattah, A. S. et al. A general approach to engineer positive-going eFRET voltage indicators. *Nat. Commun.* **11**, 3444 (2020).

28. Kannan, M. et al. Dual-polarity voltage imaging of the concurrent dynamics of multiple neuron types. *Science* **378**, eabm8797 (2022).

29. Bennett, G. J. & Xie, Y. K. A peripheral mononeuropathy in rat that produces disorders of pain sensation like those seen in man. *Pain* **33**, 87–107 (1988).

30. Devor, M. & Wall, P. D. Cross-excitation in dorsal root ganglia of nerve-injured and intact rats. *J. Neurophysiol.* **64**, 1733–1746 (1990).

31. Hanani, M. & Spray, D. C. Emerging importance of satellite glia in nervous system function and dysfunction. *Nat. Rev. Neurosci.* **21**, 485–498 (2020).

32. Dublin, P. & Hanani, M. Satellite glial cells in sensory ganglia: their possible contribution to inflammatory pain. *Brain Behav. Immun.* **21**, 592–598 (2007).

33. Hanani, M., Huang, T. Y., Cherkas, P. S., Ledda, M. & Pannese, E. Glial cell plasticity in sensory ganglia induced by nerve damage. *Neuroscience* **114**, 279–283 (2002).

34. Kim, Y. S. et al. Central terminal sensitization of TRPV1 by descending serotonergic facilitation modulates chronic pain. *Neuron* **81**, 873–887 (2014).

35. Basbaum, A. I., Bautista, D. M., Scherrer, G. & Julius, D. Cellular and molecular mechanisms of pain. *Cell* **139**, 267–284 (2009).

36. Lawson, S. N. Phenotype and function of somatic primary afferent nociceptive neurones with C-, Adelta- or Aalpha/beta-fibres. *Exp. Physiol.* **87**, 239–244 (2002).

37. Waddell, P. J. & Lawson, S. N. Electrophysiological properties of subpopulations of rat dorsal root ganglion neurons in vitro. *Neuroscience* **36**, 811–822 (1990).

38. Koerber, H. R. & Woodbury, C. J. Comprehensive phenotyping of sensory neurons using an ex vivo somatosensory system. *Physiol. Behav.* **77**, 589–594 (2002).

39. Fang, X., McMullan, S., Lawson, S. N. & Djouhri, L. Electrophysiological differences between nociceptive and non-nociceptive dorsal root ganglion neurones in the rat in vivo. *J. Physiol.* **565**, 927–943 (2005).

40. Kim, B. B. et al. A red fluorescent protein with improved monomericity enables ratiometric voltage imaging with ASAP3. *Sci. Rep.* **12**, 3678 (2022).

41. Wang, F. et al. Sensory Afferents use different coding strategies for heat and cold. *Cell Rep.* **23**, 2001–2013 (2018).

42. Yarmolinsky, D. A. et al. Coding and plasticity in the mammalian thermosensory system. *Neuron* **92**, 1079–1092 (2016).

43. St-Pierre, F. et al. High-fidelity optical reporting of neuronal electrical activity with an ultrafast fluorescent voltage sensor. *Nat. Neurosci.* **17**, 884–889 (2014).

44. Nakajima, R. & Baker, B. J. Mapping of excitatory and inhibitory postsynaptic potentials of neuronal populations in hippocampal slices using the GEVI, ArcLight. *J. Phys. D Appl. Phys.* **51**, 504003 (2018).

45. Chisholm, K. I., Khovanov, N., Lopes, D. M., La Russa, F. & McMahon, S. B. Large scale in vivo recording of sensory neuron activity with GCaMP6. *eNeuro* **5**, ENEURO.0417-17.2018 (2018).

46. Luiz, A. P. et al. Cold sensing by NaV1.8-positive and NaV1.8-negative sensory neurons. *Proc. Natl. Acad. Sci. USA* **116**, 3811–3816 (2019).

47. Ghitani, N. et al. Specialized mechanosensory nociceptors mediating rapid responses to hair pull. *Neuron* **95**, 944–954.e944 (2017).

48. Kucharczyk, M. W. et al. The impact of bone cancer on the peripheral encoding of mechanical pressure stimuli. *Pain* **161**, 1894–1905 (2020).

49. Leijon, S. C. M. et al. Oral thermosensing by murine trigeminal neurons: modulation by capsaicin, menthol and mustard oil. *J. Physiol.* **597**, 2045–2061 (2019).

50. Roome, C. J. & Kuhn, B. Simultaneous dendritic voltage and calcium imaging and somatic recording from Purkinje neurons in awake mice. *Nat. Commun.* **9**, 3388 (2018).

51. Tian, L. et al. Imaging neural activity in worms, flies and mice with improved GCaMP calcium indicators. *Nat. Methods* **6**, 875–881 (2009).

52. Dana, H. et al. Sensitive red protein calcium indicators for imaging neural activity. *Elife* **5**, e12727 (2016).

Author contributions
Y.Z. and Y.S.K. contributed to the study design with assistance from J.S., R.G., H.S., H.I., and M.L. M.C. and M.L. developed the predecessor to the ASAP4.4 voltage sensor. S.E. made and tested the ASAP4.4-Kv constructs. D.S. finalized and made the ASAP4.4 sensor. G.Z. cloned the ASAP4.4 viral constructs. M.C. made the ASAP4.4 virus. Y.S.K. contributed to data interpretation and manuscript revision. Y.Z. conceived the project and performed all experiments except where noted, and drafted the paper. R.G. and J.S. maintained, set up mating, took care of mice, and performed genotyping. R.G. assisted with GCaMP imaging work. Y.S.K. supervised all aspects of the project and wrote the paper.

Competing interests
The authors declare no competing interests.

Additional information
Supplementary information The online version contains supplementary material available at https://doi.org/10.1038/s41467-025-61774-2.

Correspondence and requests for materials should be addressed to Yu Shin Kim.

Peer review information *Nature Communications* thanks Kiryl Piatkevich and the other, anonymous, reviewer(s) for their contribution to the peer review of this work.

Reprints and permissions information is available at http://www.nature.com/reprints

Publisher's note Springer Nature remains neutral with regard to jurisdictional claims in published maps and institutional affiliations.